



# Large fluctuations of dissolved oxygen in the Indian and Pacific oceans during Dansgaard-Oeschger oscillations caused by variations of North Atlantic Deep Water subduction

Andreas Schmittner,<sup>1</sup> Eric D. Galbraith,<sup>2,3</sup> Steven W. Hostetler,<sup>4,5</sup> Thomas F. Pedersen,<sup>6</sup> and Rong Zhang<sup>7</sup>

Received 11 November 2006; revised 20 March 2007; accepted 2 April 2007; published 1 August 2007.

[1] Paleoclimate records from glacial Indian and Pacific oceans sediments document millennial-scale fluctuations of subsurface dissolved oxygen levels and denitrification coherent with North Atlantic temperature oscillations. Yet the mechanism of this teleconnection between the remote ocean basins remains elusive. Here we present model simulations of the oxygen and nitrogen cycles that explain how changes in deepwater subduction in the North Atlantic can cause large and synchronous variations of oxygen minimum zones throughout the Northern Hemisphere of the Indian and Pacific oceans, consistent with the paleoclimate records. Cold periods in the North Atlantic are associated with reduced nutrient delivery to the upper Indo-Pacific oceans, thereby decreasing productivity. Reduced export production diminishes subsurface respiration of organic matter leading to higher oxygen concentrations and less denitrification. This effect of reduced oxygen consumption dominates at low latitudes. At high latitudes in the Southern Ocean and North Pacific, increased mixed layer depths and steepening of isopycnals improve ocean ventilation and oxygen supply to the subsurface. Atmospheric teleconnections through changes in wind-driven ocean circulation modify this basin-scale pattern regionally. These results suggest that changes in the Atlantic Ocean circulation, similar to those projected by climate models to possibly occur in the centuries to come because of anthropogenic climate warming, can have large effects on marine ecosystems and biogeochemical cycles even in remote areas.

**Citation:** Schmittner, A., E. D. Galbraith, S. W. Hostetler, T. F. Pederson, and R. Zhang (2007), Large fluctuations of dissolved oxygen in the Indian and Pacific oceans during Dansgaard-Oeschger oscillations caused by variations of North Atlantic Deep Water subduction, *Paleoceanography*, 22, PA3207, doi:10.1029/2006PA001384.

## 1. Introduction

[2] Profound and rapid climatic changes characterized the North Atlantic region during much of the last ice age, as first revealed by oscillations in the oxygen isotope composition ( $\delta^{18}\text{O}$ , a proxy for local air temperature) of Greenland ice cores [Dansgaard et al., 1982; Oeschger et al., 1984]. These so-called Dansgaard-Oeschger (D-O) oscillations were most likely associated with instabilities of the Atlantic meridional overturning circulation, such that North Atlantic Deep Water (NADW) subduction and northward oceanic heat transport was reduced during cold (stadial) episodes

and enhanced during mild (interstadial) phases [Broecker et al., 1985]. This interpretation is buttressed by numerous model studies [Bryan, 1986; Schmittner et al., 2003] and observational data [Charles and Fairbanks, 1992; Bond et al., 1993; Sarnthein et al., 2001; Piotrowski et al., 2005]. Paleoclimatographic records of sufficiently high temporal resolution are still relatively sparse outside of the North Atlantic [Voelker, 2002]. However, during the last decade a more detailed picture has begun to emerge of the expression of D-O oscillations in the Indian and Pacific oceans. Assessing and understanding the remote impacts of the Atlantic meridional overturning circulation is of particular importance, given that projections of future climate change show the possibility for substantial weakening or even complete shut down of the circulation in the centuries to come [Manabe and Stouffer, 1993; Schmittner et al., 2005a] and given suggestions that such weakening has already begun [Bryden et al., 2005].

[3] Correlations of fluctuations in the northeast Pacific oxygen minimum zone with Greenland ice core  $\delta^{18}\text{O}$  were first identified about 10 years ago in records of alternating laminated and bioturbated sediments in the Santa Barbara Basin [Kennett and Ingram, 1995; Behl and Kennett, 1996]. Multiple records throughout the midlatitude and low-latitude northeast Pacific [Cannariato and Kennett, 1999; Zheng et al., 2000; Kienast et al., 2002; van Geen et al.,

<sup>1</sup>College of Oceanic and Atmospheric Sciences, Oregon State University, Corvallis, Oregon, USA.

<sup>2</sup>Department of Earth and Ocean Sciences, University of British Columbia, Vancouver, British Columbia, Canada.

<sup>3</sup>Now at Atmospheric and Oceanic Sciences, Princeton University, Princeton, New Jersey, USA.

<sup>4</sup>U.S. Geological Survey, Corvallis, Oregon, USA.

<sup>5</sup>Department of Geosciences, Oregon State University, Corvallis, Oregon, USA.

<sup>6</sup>School of Earth and Ocean Sciences, University of Victoria, Victoria, British Columbia, Canada.

<sup>7</sup>Geophysical Fluid Dynamics Laboratory, Princeton University, Princeton, New Jersey, USA.

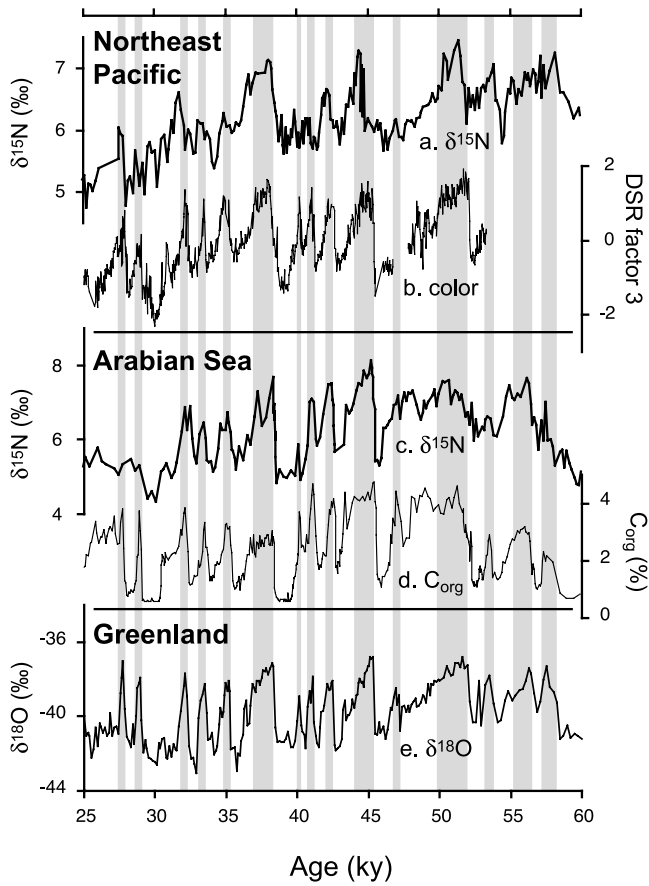


**Figure 1.** High-resolution records from the last glacial period (60–25 kyr B.P.) from the (a and b) Pacific and (c and d) Indian oceans indicating apparently synchronous fluctuations of subsurface oxygen levels and biological productivity with (e) Greenland climate. Nitrogen isotopes from *Hendy et al.* [2004] (ODP site 1017, Figure 1a) and *Ivanochko et al.* [2005] (NIOP site 905, Figure 1d) record changes in water column denitrification, which is controlled by the intensity of suboxia ( $<5 \mu\text{M}$  oxygen) such that high values of  $\delta^{15}\text{N}$  indicate more denitrification and, by inference, lower oxygen concentrations. Sediment color (core MV99-PC08, Figure 1b [*Ortiz et al.*, 2004]) and organic carbon content (core SO90-136KL, Figure 1d [*Schulz et al.*, 1998]) are interpreted to record increased productivity during warm periods in Greenland, which are shown by higher oxygen isotopes values (Figure 1e). All records are plotted on their original, published age scales.

2003; *Hendy and Kennett*, 2003; *Crusius et al.*, 2004; *Ortiz et al.*, 2004; *Hendy et al.*, 2004; *McKay et al.*, 2005] and the Arabian Sea [*Schulz et al.*, 1998; *Schulte et al.*, 1999; *Reichart et al.*, 1998; *Suthhof et al.*, 2001; *Altabet et al.*, 2002; *Reichart et al.*, 2002; *Higginson et al.*, 2004; *Reichart et al.*, 2004; *Ivanochko et al.*, 2005] now reveal temporal fluctuations of thermocline oxygen concentrations similar to

those from the Santa Barbara Basin, suggesting a tight coupling of all these regions to the North Atlantic (Figure 1).

[4] The determination of leads or lags between the oxygen fluctuations and those of Greenland temperature is limited to the accuracy of radiocarbon dating ( $\sim 200$  years) during the deglacial Heinrich event 1–Bølling–Ållerød–Younger Dryas–Holocene oscillation [*Kennett and Ingram*, 1995]. Before this, the age models are even more poorly constrained, and in many cases rely on extending the observed correlation during the deglaciation to the older sections (wiggle matching). Nonetheless, the widespread coherence of the observations, combined with ancillary data, convinced the authors of these works that the oceanic changes were roughly coeval with the changes in Greenland temperature. The higher stadial dissolved oxygen concentrations are paralleled by evidence for decreased export production (Figure 1), suggesting that a mechanistic coupling between biological productivity in these regions and the North Atlantic contributed to the changes in subsurface oxygen concentrations. Note that some productivity proxies (e.g., total organic carbon) may also be influenced by changes in preservation in the sediments where the relative proportions of refractory and labile organic matter vary. Unlike labile organic matter, refractory organic compounds can be preferentially preserved under anoxic conditions in sediments [e.g., *Ganeshram et al.*, 1999].

[5] Identification of a unifying mechanism that explains these joint responses, thus an implied underlying teleconnection, remains a challenge. Most hypotheses call for changes in atmospheric circulation with attendant change in the monsoons of the Indian Ocean region [*Schulz et al.*, 1998; *Reichart et al.*, 1998; *Suthhof et al.*, 2001; *Altabet et al.*, 2002; *Reichart et al.*, 2002; *Higginson et al.*, 2004; *Reichart et al.*, 2004; *Ivanochko et al.*, 2005] and changes in the trade winds or local winds in the Pacific [*Mikolajewicz et al.*, 1997; *Hendy and Kennett*, 2003; *Hendy et al.*, 2004] that ultimately affect ocean circulation and productivity in the immediate vicinity of the subsurface oxygen minima. Using a zonally averaged model *Schulte et al.* [1999] suggested an oceanic teleconnection for the Indian Ocean. Here we present for the first time detailed, three-dimensional ocean simulations of oxygen and nitrogen cycling during idealized D–O oscillations. Our results suggest a parsimonious and unifying explanation can be found in the impact of the buoyancy-driven ocean circulation on productivity and subsurface nutrient and oxygen distributions.

## 2. Present-Day Distribution of Dissolved Oxygen in the Ocean

[6] Dissolved oxygen concentrations vary dramatically in the ocean, particularly in the thermocline, where they span a range from supersaturated to undetectable (Figures 2a, 3a, and 3b). The saturation solubility of oxygen is higher in cold seawater. Surface waters are near saturation with respect to oxygen while, below, oxygen concentrations are diminished by the respiration of organic matter. The subsurface distribution of oxygen is hence determined by a balance between supply, which depends on the efficiency with which oxygen-rich surface waters are mixed and

transported toward the ocean interior, and consumption, which is controlled by biological production at the sunlit surface and subsequent sinking of dead organic matter. Because productivity depends on nutrient input to the photic zone, both oxygen supply and consumption ultimately depend on ocean circulation. In the so-called shadow zones of the global ocean, i.e., the Arabian Sea in the northern Indian ocean, and the eastern tropical North and South Pacific, oxygen concentrations are so low (below about  $5 \mu\text{M}$ , see Figure 2a) that specialized microbes use nitrate as an electron acceptor instead of oxygen in order to remineralize organic compounds. This process, called denitrification, reduces nitrate to  $\text{N}_2$  gas, and preferentially consumes nitrate with the light isotope  $^{14}\text{N}$ , enriching the residual nitrate in the heavy isotope  $^{15}\text{N}$  (thus imparting a higher  $\delta^{15}\text{N}$ ). Once the high  $\delta^{15}\text{N}$  nitrate wells up to the surface it is incorporated in organic matter by plankton, remains of which can be found in ancient ocean sediments. Thus sedimentary  $\delta^{15}\text{N}$  records the strength of denitrification. In locations proximal to denitrifying zones, bulk sedimentary  $\delta^{15}\text{N}$  provides an excellent monitor of the extent of suboxia in the past (e.g., Figures 1a and 1c).

[7] We use the UVic Earth System Climate Model Version 2.7, which includes an improved version of a simple ocean ecosystem model with two phytoplankton classes (nitrogen fixers and other phytoplankton), two nutrients ( $\text{NO}_3$  and  $\text{PO}_4$ ) as well as explicit representations of denitrification in the water column and nitrogen fixation. Nitrogen

fixers are not limited by nitrate because they are able to fix nitrogen from dissolved  $\text{N}_2$  gas, but they have lower growth rates than other phytoplankton. (A more detailed model description is given in the Appendix.)

[8] Our model captures the main features of the observed modern oxygen distribution (Figures 2a and 2b and 3a–3d). For example, on the  $\sigma_\theta = 26.8 \text{ kg m}^{-3}$  density surface (Figures 2a and 2b), oxygen concentrations are highest ( $>250 \mu\text{M}$ ) in the high-latitude outcrop areas of the Southern Ocean and North Atlantic as well as in the northwest Pacific where intermediate waters are ventilated. Oxygen concentrations decrease as these subpolar mode waters subduct into the thermocline and travel toward lower latitudes. Lowest concentrations ( $<5 \mu\text{M}$ ) are found in the eastern tropical Pacific and Atlantic as well as in the northern Indian Ocean. Owing to insufficiently resolved tropical dynamics [Toggweiler *et al.*, 1991; Aumont *et al.*, 1999; Large *et al.*, 2001] the model simulates very large suboxic zones in the eastern tropical Pacific and hence overestimates denitrification there ( $90$  versus  $\sim 50 \text{ Tg N yr}^{-1}$  observed [Deutsch *et al.*, 2001]). In the northern Indian Ocean, suboxic conditions occur in the modeled Bay of

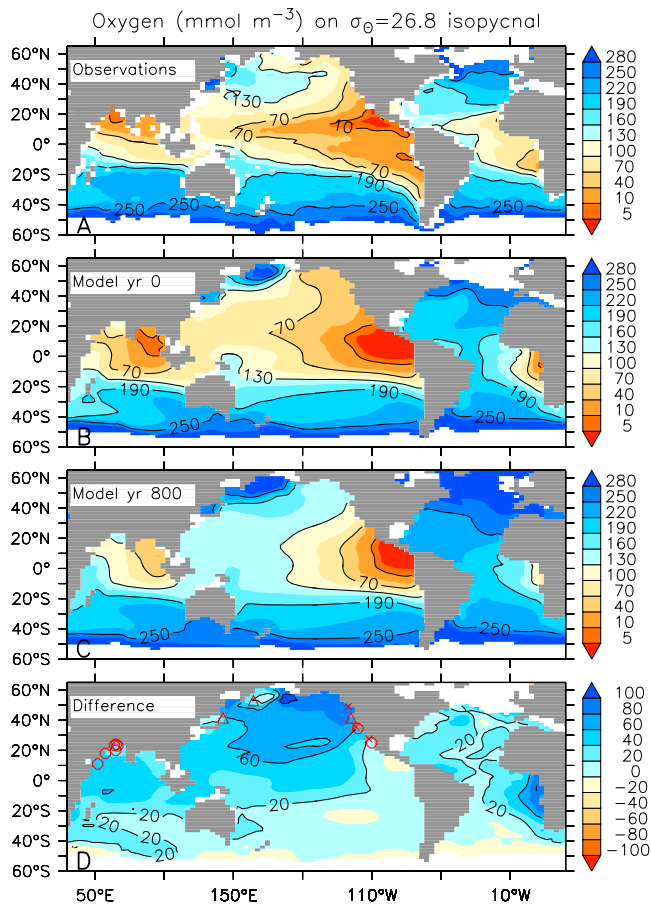


**Figure 2.** Oxygen concentrations on the  $\sigma_\theta = 26.8$  isopycnal surface corresponding to subpolar mode water. This density surface is currently located between about 200 and 700 m depth at midlatitudes and low latitudes both in present-day observations and in the model and deepens in the stadial simulation by  $\sim 50$  m (not shown). (a) General patterns apparent in the observations [Levitus and Boyer, 1994] reproduced in the control simulation (b) including higher oxygen concentrations in the Atlantic than in the Pacific, highest oxygen concentrations at high latitudes, and lowest values in the equatorial east Pacific, the northern Indian Ocean, and the equatorial east Atlantic. Differences between the model and the observations are caused by model biases such as coarse resolution and underestimation of the eastward flowing equatorial undercurrents, which transport oxygenated waters into the oxygen-depleted eastern equatorial regions. Thus modeled suboxic zones in the eastern equatorial Pacific are overestimated. In the Indian Ocean, suboxic conditions are found in the Bay of Bengal rather than in the Arabian Sea. (c) At model year 800 after NADW formation stopped, oxygen concentrations increased almost everywhere, and the volume of suboxic water strongly reduced. (d) Higher oxygen concentrations particularly pronounced north of about  $20^\circ\text{S}$  in the Indian and Pacific oceans. Red symbols in (Figure 2d) show sites of sediment cores in which increased subsurface oxygen levels have been observed during stadials of marine isotope stage 3 (circles) [Kennett and Ingram, 1995; Behl and Kennett, 1996; Cannariato and Kennett, 1999; Kienast *et al.*, 2002; van Geen *et al.*, 2003; Hendy and Kennett, 2003; Ortiz *et al.*, 2004; Hendy *et al.*, 2004; Schulz *et al.*, 1998; Suthhof *et al.*, 2001; Altabet *et al.*, 2002; Ivanochko *et al.*, 2005; Pourmand *et al.*, 2004; Reichert *et al.*, 2004; Mix *et al.*, 1999; Schulte *et al.*, 1999] or during the deglaciation (crosses) [McKay *et al.*, 2005; Zheng *et al.*, 2000] and sites of decreased productivity during deglacial stadials (triangles) [Crusius *et al.*, 2004; Mix *et al.*, 1999].

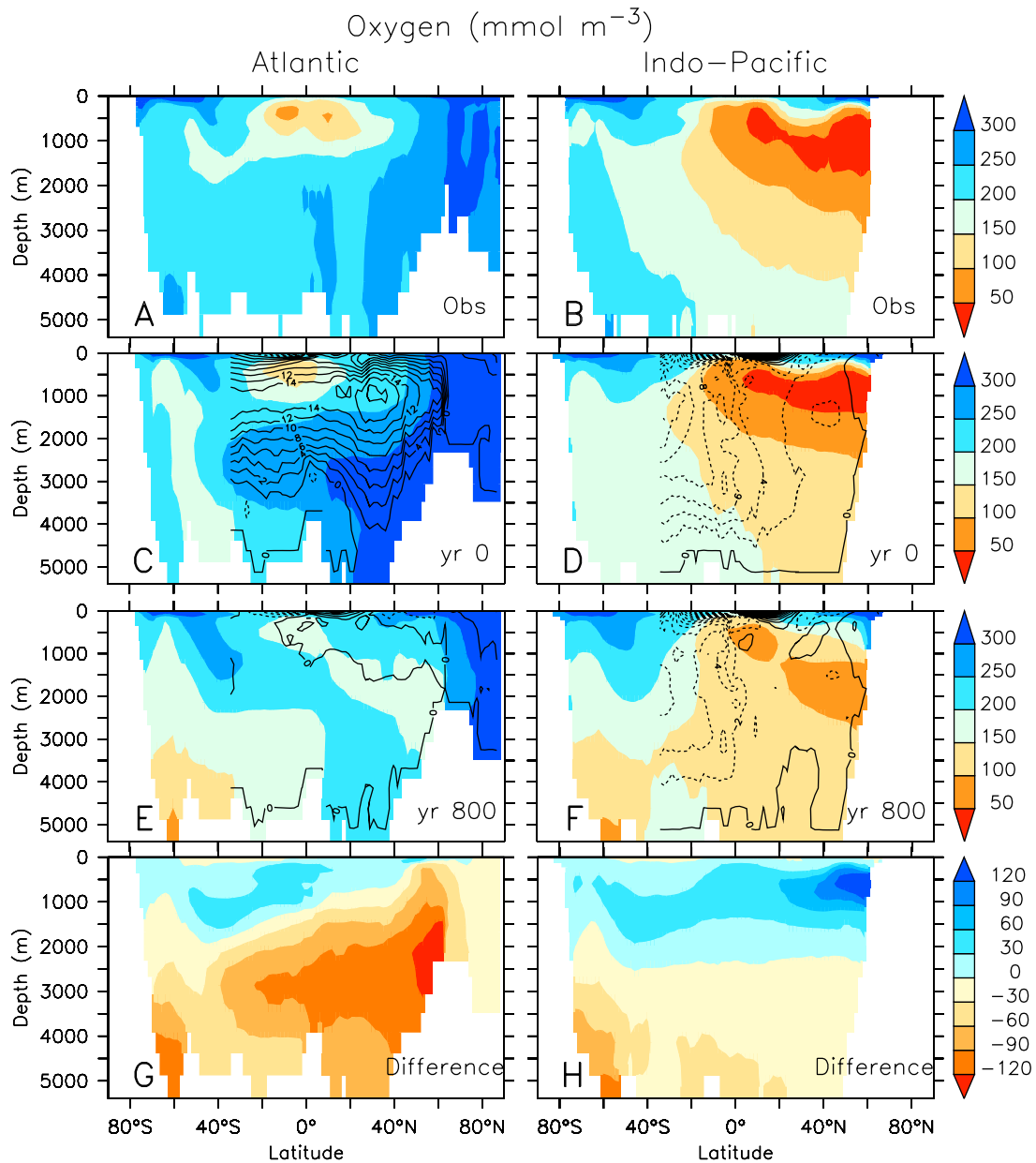


**Figure 3.** Zonally averaged oxygen concentrations (color scale) in the (left) Atlantic and (right) Indo-Pacific. (a and b) Observations from *Levitus and Boyer* [1994]. Highest oxygen concentrations (blue colors) are found in high-latitude surface waters and in deep waters of the North Atlantic. As NADW propagates south, respiration of organic matter removes dissolved oxygen. The lowest concentrations (orange colors) in deep waters are found in the North Pacific. (c and d) Results from the present-day simulation with model version sNPs reproducing the observed pattern. Isolines of the Eulerian meridional overturning stream function in Figures 3c–3f illustrate the zonally integrated flow. Positive values (solid lines) denote clockwise circulation; negative values (dashed lines) denote counterclockwise circulation. Isoline difference is 2 Sv ( $1 \text{ Sv} = 10^6 \text{ m}^3 \text{ s}^{-1}$ ). (e and f) Reduced NADW production leading to decreased oxygen concentrations in the (g) deep North Atlantic and increased values in the upper ocean, particularly in the (h) Indo-Pacific.

Bengal rather than in the Arabian Sea, apparently because of an incorrect partitioning of thermocline nutrients between the basins. The modeled distribution of oxygen in the deep sea agrees well with observations (Figures 3a–3d). The meridional overturning circulation creates large interbasin

differences in oxygen concentrations of deep waters. In the North Atlantic, deep waters have high oxygen concentrations ( $>250 \mu\text{M}$ ) because they have been recently downwelled from the high-latitude surface. In the North Pacific, deep waters have very low oxygen concentrations because



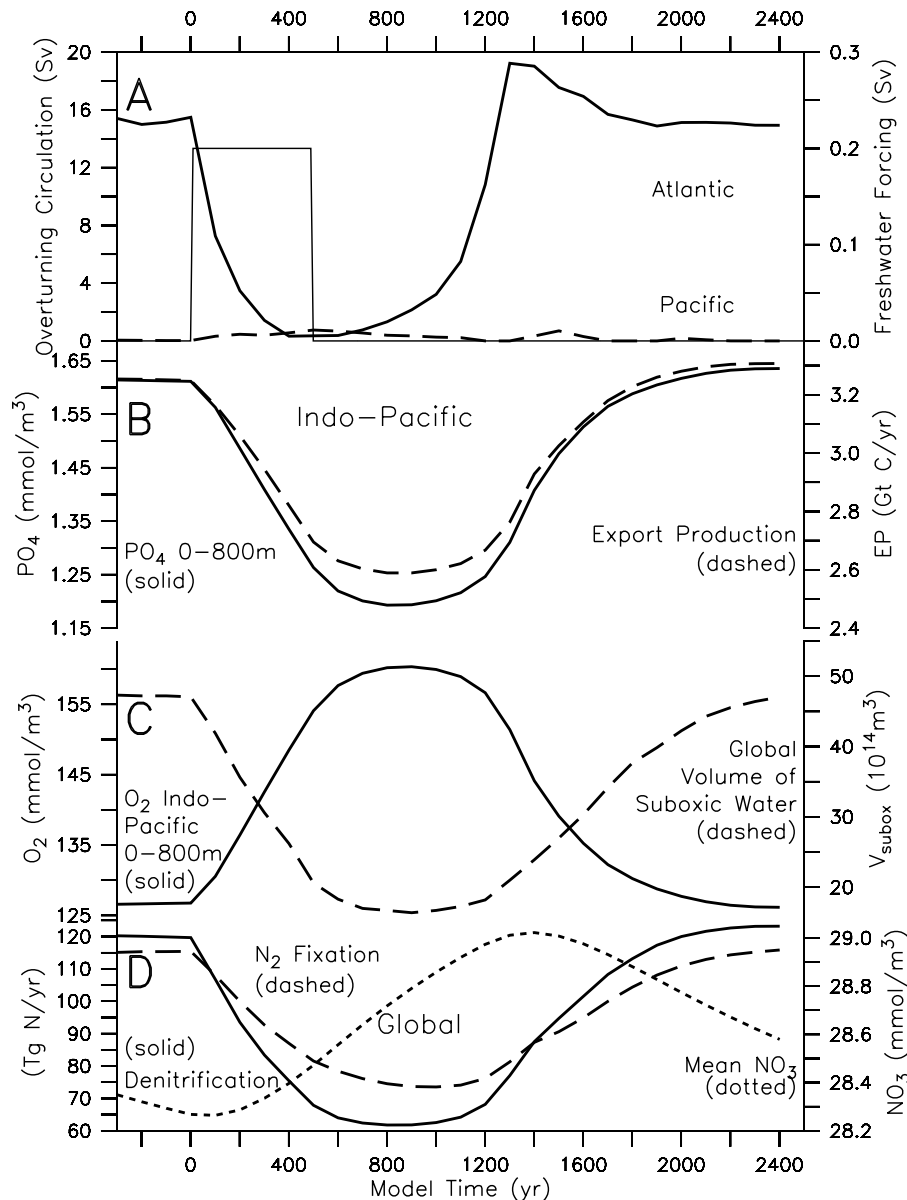


**Figure 4.** Simulation of a Dansgaard-Oeschger event with the standard model version (sNPs). (a) A freshwater perturbation applied in the North Atlantic between  $35^{\circ}$  and  $70^{\circ}\text{N}$  (thin line, right scale) causing a disruption of the overturning circulation in the Atlantic (solid line, left scale) and a slight increase of the circulation in the North Pacific (dashed line, left scale). (b) Average upper ocean nutrient ( $\text{PO}_4$ ) concentrations (solid line, left scale) and integrated export production (dashed line, right scale), calculated as the sinking of particulate organic carbon across 120 m depth in the Indo-Pacific north of  $35^{\circ}\text{S}$ . (c) Average upper ocean oxygen ( $\text{O}_2$ ) concentrations (solid line, left scale) and volume of suboxic water (dashed line, right scale) in the Indian and Pacific oceans. (d) Global rates of denitrification (solid line, left scale) and nitrogen fixation (dashed line, left scale) and global mean nitrate concentration (dotted line, right scale).

they have been isolated from the atmosphere for a long time, during which respiration of organic matter has removed much of the original oxygen.

### 3. Simulations of Dansgaard-Oeschger Events

[9] Wind velocities were kept fixed in the simulation shown in Figures 2–4 in order to isolate the effect of

changes in the buoyancy-forced ocean circulation. The effect of changes in the wind-driven circulation is addressed in section 5. Changes in deepwater formation are triggered by applying a perturbation to the surface freshwater balance in the North Atlantic for 500 years (Figure 4) similar to previous studies [Schmittner *et al.*, 2003]. Deepwater formation in the North Atlantic ceases for  $\sim 1000$  years as a response to this freshwater forcing and subsequently returns

to its initial state. The simulated response of the climate system, characterized by strong cooling and increased sea ice cover in the North Atlantic (particularly in winter) and warming of thermocline waters in the Southern Hemisphere (not shown), is consistent with paleoclimate proxy records of stadial conditions [Schmittner *et al.*, 2003].

[10] In agreement with a previous model study [Schmittner, 2005], reduced supply of deep nutrient-rich waters to the Indian and Pacific euphotic zones leads to a decline of export production by about 30% in the stadial simulation. Figure 4c shows that this is accompanied by a strong increase of upper ocean oxygen concentrations. The volume of suboxic water decreases dramatically, by about 80%. Consequently, global denitrification in the water column is reduced by more than one half. Less denitrification leads to higher N/P ratios in upwelling waters, reducing the competitive fitness of nitrogen fixers and, hence global nitrogen fixation decreases in tandem. The decrease in nitrogen fixation is slightly less than that of denitrification, such that the globally averaged nitrate concentration increases by  $\sim 1.1 \mu\text{M}$  (i.e.,  $\sim 4\%$ ). The response of the suboxic zones and the nitrogen cycle (denitrification and nitrogen fixation) might be overestimated by the model because of the overestimation of the suboxic zones in the eastern tropical Pacific in the present-day simulation. Nonetheless, the response is qualitatively robust in different model formulations, with changes wrought by the meridional overturning overwhelming other factors (see also sensitivity experiments in the following section).

[11] Owing to the weakened meridional overturning circulation, the interbasin difference in deepwater oxygen concentrations is reduced dramatically during the stadial (Figures 3e and 3f). Oxygen concentrations decrease strongly in deep waters of the Atlantic and in the Southern Ocean below about 1 km depth (Figures 3g and 3h) because of reduced advection of NADW. Upper ocean oxygen concentrations increase almost everywhere, particularly in the Northern Hemisphere of the Indian and Pacific oceans (Figures 2d, 3g, and 3h). The model results are consistent with available paleorecords from the Indian and northeast Pacific as illustrated in Figure 2d. Note that most paleorecords only indicate the sign of the change and cannot be used for a quantitative comparison. Simulated oxygen variations near the Santa Barbara Basin and in the Arabian Sea show little (compared with the uncertainties in the age models) time lag (200–400 years) between the overturning and climate changes in the North Atlantic (Figure 4) consistent with the proxy record. Simulated transitions between stadial and interstadial conditions occur on multicentennial (300–400 years) timescales. This timescale is consistent with, although somewhat slower than, an estimate (200 years) from a high-resolution record in the Arabian Sea [Higginson *et al.*, 2004]. Additional local factors, not accounted for in our idealized experiment, may accentuate the rapidity of the transitions. For instance, on the basis of faunal assemblages Reichert *et al.* [1998, 2002, 2004] suggested that the mixed layer in the Arabian Sea was deeper during stadial periods. These mechanisms would have also contributed to better oxygenation of subsurface waters there. However, we cannot

confirm this mechanism from our model results, which show little changes in stratification.

[12] The model response also presents an explanation for the millennial ice core record of atmospheric nitrous oxide [Flueckiger *et al.*, 2004] which shows lower concentrations during stadials. Oxygen minimum zones are one of the major sources of  $\text{N}_2\text{O}$  [Gruber, 2004], and the dramatic expansions of global suboxic waters under interstadial conditions simulated here could have contributed to the observed interstadial increases in  $\text{N}_2\text{O}$ , although there are also important terrestrial and open ocean sources that might have been involved. We note that a new records of sedimentary  $\delta^{15}\text{N}$  from the southeast Pacific suggests a temporal pattern of denitrification distinct from those from the Northern Hemisphere [Martinez *et al.*, 2006; Robinson *et al.*, 2007]. Given the much smaller amplitude of the model response in the Southern Hemisphere (Figure 2d), it seems plausible that a different mechanism controls fluctuations of the suboxic zones there. This would not be inconsistent with our simulations.

[13] The results presented above suggest that changes in the buoyancy forced ocean circulation can cause large variations in subsurface oxygen levels via changing oxygen demand, a mechanism so far neglected in hypotheses of oxygen fluctuations on millennial timescales. Other mechanisms proposed for the observed increase in stadial oxygen concentrations include changes in North Pacific Intermediate Water (NPIW) formation [Kennett and Ingram, 1995; Behl and Kennett, 1996; Zheng *et al.*, 2000] and changes in wind-driven ocean circulation [Kienast *et al.*, 2002; Hendy and Kennett, 2003; Schulz *et al.*, 1998; Suthhof *et al.*, 2001; Altabet *et al.*, 2002; Ivanochko *et al.*, 2005; Mikolajewicz *et al.*, 1997]. In order to quantify these effects we designed five additional sensitivity experiments.

#### 4. Ventilation Versus Consumption

[14] First, the freshwater perturbation experiment was repeated with a model version with fixed interior oxygen sinks, analogous to the approach of Meissner *et al.* [2005]. Thus oxygen demand does not change and the simulated anomalies are exclusively due to changes in supply (ventilation including changes in air sea gas exchange). As shown in Figures 5 and 6 both ventilation and consumption changes are important. Increased ventilation dominates the total oxygen response in the North Pacific (e.g., in the vicinity of the Santa Barbara Basin), whereas consumption changes are more important at low latitudes such as in the Arabian Sea. Increases in ventilation seen in the North Pacific and Indian oceans in Figure 6b are confirmed by higher radiocarbon concentrations there by about 20‰ (not shown). Ultimately, they are caused by deepening of mixed layers and steepening of isopycnals in the Southern Ocean and North Pacific related to salinification of the upper ocean and freshening of the deep sea owing to the missing injection of salty NADW into the deep [Schmittner *et al.*, 2007].

[15] In order to further explore the role of changes in NPIW formation a model version with a stronger response of NPIW to the forcing in the North Atlantic has been constructed. This was achieved through weakening the

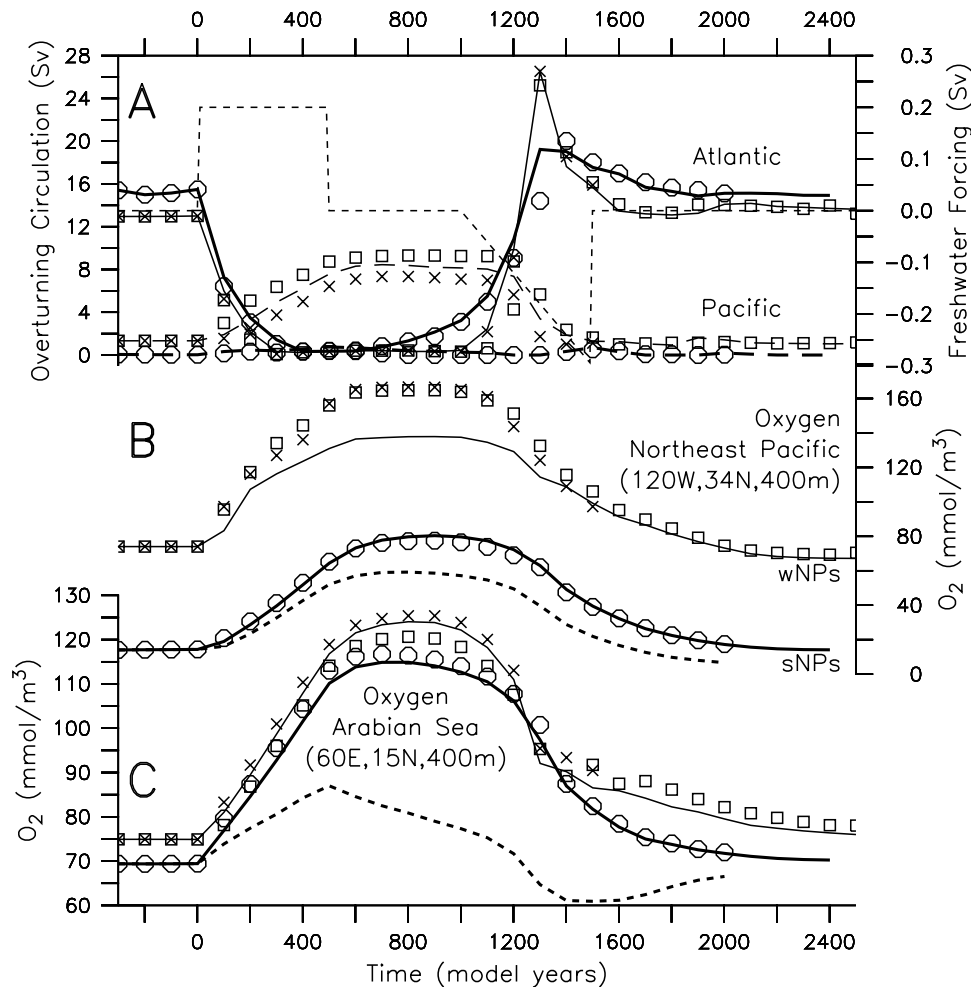


**Figure 5.** Sensitivity experiments. Five different experiments were performed in order to unravel the influence of ventilation versus oxygen consumption, stratification in the North Pacific, and changes in wind-driven circulation on millennial oxygen variations: the standard experiment with strong North Pacific stratification (sNPs, thick solid lines), the same experiment but with fixed oxygen consumption (thick dotted lines), the same as the standard experiment but with weak North Pacific stratification (wNPs, thin solid lines), two runs with stadial wind stress anomalies from the GENESIS and GFDL models applied during years 0–1000 with model version wNPs (wNPs plus GENESIS wind (squares), wNPs plus GFDL wind (crosses)), and finally a simulation with the GFDL wind stress anomalies applied to model sNPs (sNPs plus GFDL wind (circles)). (a) Freshwater forcing (thin dashed line) in the North Atlantic for experiments with model version wNPs, overturning in the Atlantic (solid line) and overturning in the Pacific (dashed line). Oxygen concentrations in the (b) northeast Pacific in the vicinity of the Santa Barbara Basin and (c) Arabian Sea.

background stratification in the North Pacific by manipulating its surface freshwater balance. Specifically, a 0.1 Sv freshwater input to the North Pacific north of 40°N, which was used as a constant flux correction (and compensated for in the rest of the world ocean) in the standard simulation (sNPs), has been removed. This experiment is motivated by reconstructions suggesting reduced stratification in the glacial North Pacific [Keigwin, 1998]. Note that the Atlantic overturning in the weak North Pacific stratification model version (wNPs) is bistable. That is, both the NADW “on” and “off” states are stable steady states without perturbation (in contrast to model version sNPs which is monostable

such that only the NADW “on” state is stable). Therefore, in order to force NADW resumption, freshwater was extracted from the North Atlantic after year 1000, increasing linearly until year 1500 (Figure 5).

[16] In this model version there is a strong increase of NPIW formation (Figure 5a) in response to weakened NADW flow, consistent with the Atlantic-Pacific seesaw mechanism [Saenko *et al.*, 2004]. This experiment also confirms an earlier study demonstrating that the response of NPIW to perturbations of NADW is highly sensitive to stratification in the North Pacific [Schmittner and Clement, 2002]. However, despite the strong increase

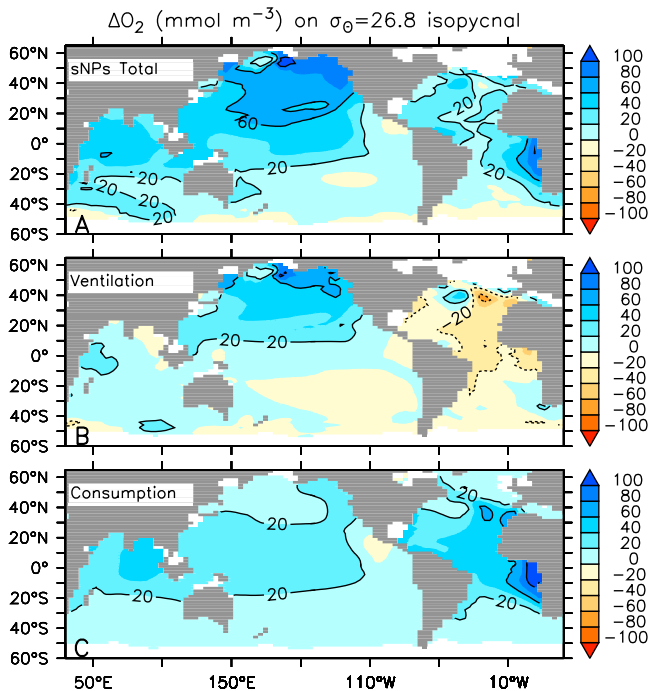


**Figure 6.** Oxygen anomaly on  $\sigma_{\theta} = 26.8$  isopycnal surface at model year 800 as in Figure 2d. (a) Total anomaly (same as Figure 2d). (b) Anomaly due to ventilation changes only (experiment with constant interior oxygen sinks). (c) Anomaly due to consumption changes only (values of Figure 6a minus values of Figure 6b).

in NPIW formation, the response of subsurface oxygen concentrations in the northeast Pacific is smaller than in the case without strong NPIW changes (compare Figure 7a with Figure 2d). Further analysis of this experiment shows that the changes in oxygen demand in the North Pacific are similar to those in experiment sNPs. This suggests a nonlinear response in that the effect of increased mixed layer depths and ventilation on oxygen concentrations in the North Pacific is stronger in model sNPs than in model wNPs despite the larger changes in the meridional overturning circulation in the North Pacific in model wNPs. We conclude that the large oxygen response is robust with respect to a different background stratification in the North Pacific.

## 5. Influence of Wind-Driven Ocean Circulation Changes

[17] Additional sensitivity experiments were designed to quantify the role of wind-driven ocean circulation changes by adding stadial wind stress anomalies computed from Atmospheric General Circulation Models (AGCMs). Two simulations with GENESIS [Thompson and Pollard, 1997], each integrated for 20 years, were performed with monthly SST and sea ice boundary conditions taken from the UVic model version wNPs (see Figure 8), one using the end of the control run (year 0 in Figure 4) and the other one using year

800 of the stadial simulation. The differences between the simulated monthly averaged wind stress fields from the two GENESIS runs were then added as an anomaly (Figure 8b) to the wind stress field used to drive the UVic model between years 0 and 1300. In this simulation an anomalous anticyclonic gyre over the North Pacific leads to increased northeasterly winds over the Gulf of Alaska (Figure 8b) increasing ocean convection and ventilation there. This interpretation is based on anomalous cold, fresh, high  $\Delta^{14}\text{C}$  (younger) and more oxygenated waters there at 300–900 m depth (not shown) and consistent with increased NPIW formation (Figure 5a). This anomaly is advected south with the mean circulation. Consequently, the stadial oxygen increase in the vicinity of the Santa Barbara Basin is almost 50% larger compared to the simulation with constant winds (Figure 5b). This supports the notion that changes in wind-driven ocean circulation can cause significant changes in oxygen concentrations.

[18] The simulated response of wind stress changes in the North Pacific depends on the SST anomaly. Model version wNPs shows a strong warming there (Figure 8b), whereas model version sNPs shows a much weaker response because of more stable background stratification (Figure 8c). Some coupled models predict a cooling of the North Pacific [Mikolajewicz et al., 1997; Zhang and Delworth, 2005] with an increased Aleutian low as a response to a collapse of the

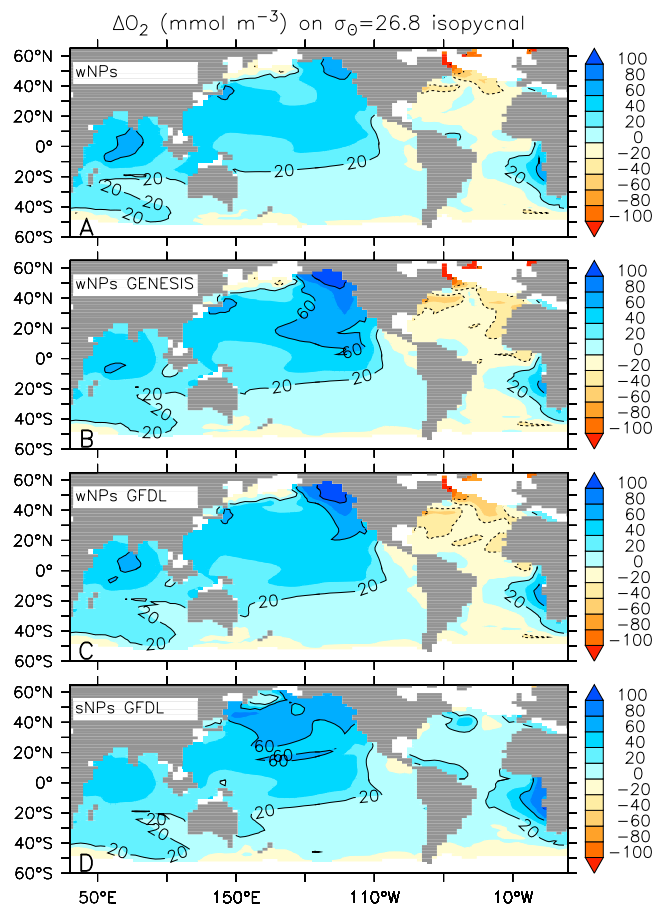


**Figure 7.** Same as Figure 2d but for the different sensitivity experiments.



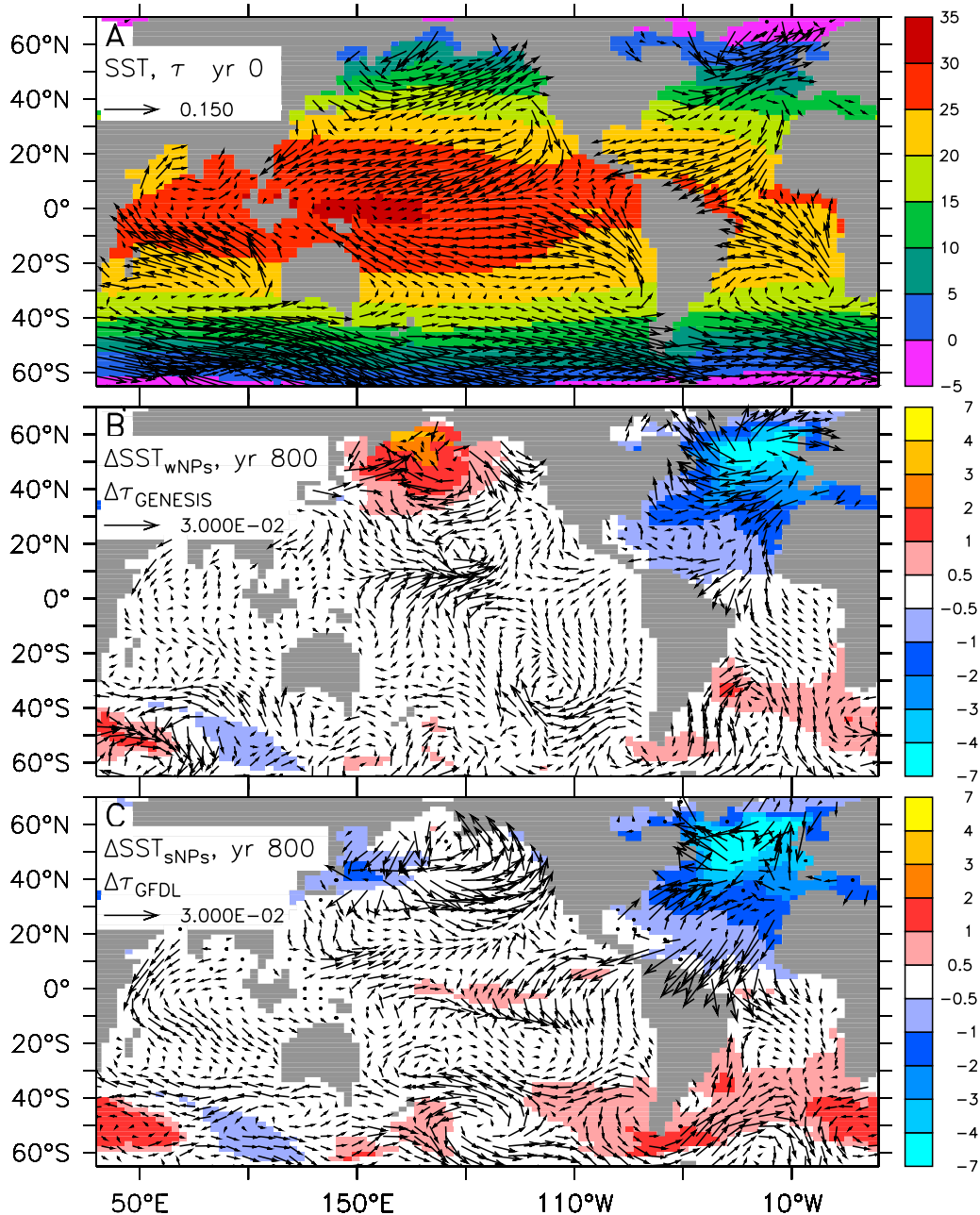


**Figure 8.** (a) Annual mean sea surface temperature ( $^{\circ}\text{C}$ ) of the control simulation at year 0, (b) stadal anomalies at year 800 for model version wNPs (without GENESIS wind stress anomalies), and (c) sNPs plus GFDL wind. Arrows show wind stress (Pa) for the control run (Figure 8a) and anomalies as obtained from the GENESIS model (Figure 8b) forced with the SST anomalies shown in (Figure 8b) and anomalies from the GFDL model (Figure 8c). Note that the length scale for the wind stress anomaly (indicated by the arrow in the top left corner) in Figures 8b and 8c is only 20% of that in Figure 8a.

Atlantic overturning whereas others show a warming [Mikolajewicz *et al.*, 2007]. Paleoreconstructions tentatively (given age uncertainties) seem to support warming [Sarnthein *et al.*, 2006] consistent with a weaker stratification during glacial times [Keigwin, 1998]. However, in order to account for the uncertainties additional experiments were conducted in which wind stress anomaly fields from the GFDL model [Zhang and Delworth, 2005] were used, which simulates a cooler North Pacific and a cyclonic

wind stress anomaly there (Figure 8c). Note, however, that the coupled GFDL model was only integrated for 60 years and the deep ocean interior is far from equilibrium. Nevertheless, except for the North Pacific, both models broadly agree in the simulated wind stress anomaly patterns, with the GFDL model displaying generally somewhat larger amplitudes than GENESIS.

[19] Figures 7c and 7d show the resulting oxygen anomalies from simulations with GFDL wind stress anomalies

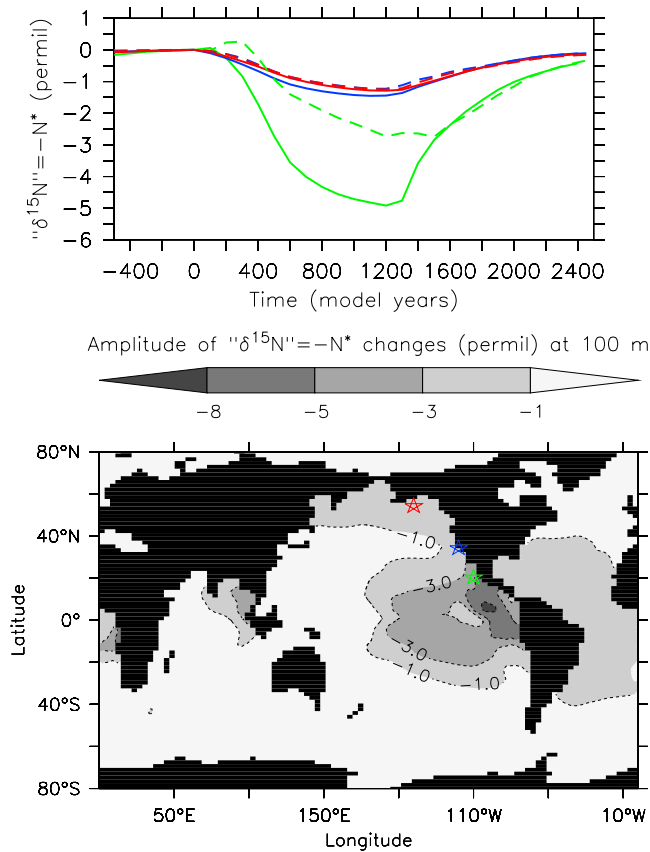


**Figure 9.** Estimated amplitude of  $\delta^{15}\text{N}$  changes. (top) Time series at the locations of the stars in Figure 9b. (bottom) Spatial pattern of  $\delta^{15}\text{N}$  amplitude at 100 m depth. Sites of records in the east Pacific are indicated by the stars (blue, site 1017, see Figure 1a; red, site 887; and green, a site closer to the denitrification zones for comparison with records from the Arabian Sea, see Figure 1c). Solid lines correspond to the standard simulation (sNPs), and dashed lines correspond to model wNPs.

applied to both model versions wNPs and sNPs. These results confirm our earlier assessment that generally the anomalies brought about by changes in the wind-driven circulation are considerably smaller than those resulting from the buoyancy-driven circulation. Largest effects due to the GFDL wind stress anomalies occur in the northeast Pacific where oxygen increases are enhanced in model version wNPs (compare Figure 7c with Figure 7a) consistent with the results from GENESIS (Figure 7b). This surprisingly similar response to the very different wind stress anomalies from GFDL and GENESIS is due to a similar response of the near surface ocean circulation along the south coast of Alaska with enhanced westerly flow (not shown) indicating nonlocal response. Both simulations show increased convergence of surface flow and reduced stratification in the Gulf of Alaska, warmer and more saline surface waters, cooling and freshening between 200 and 800 m depth and a reduced vertical radiocarbon gradient, all indications of increased downwelling, winter convection and ventilation of intermediate waters there. Interestingly

in model version sNPs the GFDL wind stress anomalies lead to smaller oxygen increases (compare Figure 7d with Figure 2d) demonstrating that the effect of the same wind stress anomalies on subsurface oxygen concentrations can depend qualitatively on the background stratification. The reason is likely lower vulnerability to convection due to more stable stratification.

[20] In the Indian Ocean the influence of wind stress on subsurface oxygen concentrations (Figures 6c and 7) in our simulations is negligible despite a reduced stadial Indian summer monsoon simulated by GENESIS as well as by the GFDL model, consistent with other model results [Timmermann *et al.*, 2005]. This indicates that changes in wind-driven circulation did not have a large impact on the observed stadial-interstadial oxygen oscillations in the Arabian Sea contrary to previous hypotheses [Schulz *et al.*, 1998; Suthhof *et al.*, 2001; Altabet *et al.*, 2002; Ivanochko *et al.*, 2005]. However, the fact that the simulated oxygen minimum in the Arabian Sea is too weak is a matter of concern, possibly affecting the reliability of the simulated effects of monsoonal changes on subsurface oxygen concentrations there.

## 6. Estimating $\delta^{15}\text{N}$ Changes

[21] Our model does not include an explicit treatment of nitrogen isotopes. However, a zero-order approximation to  $\delta^{15}\text{N}$  can be obtained by considering that water column denitrification has the same effect on  $\delta^{15}\text{N}$  as on  $N^* = \text{NO}_3 - 16 \cdot \text{PO}_4$  [Gruber, 2004]. We thus approximate  $\delta^{15}\text{N} = -N^*$ . This approach neglects all other processes affecting  $\delta^{15}\text{N}$  such as variations in sedimentary denitrification and relative nitrate consumption. However, it allows a first test as to whether the simulated magnitude of denitrification changes is consistent with the observed  $\delta^{15}\text{N}$  amplitude. The model predicts  $\delta^{15}\text{N}$  changes between 2–5‰ close to the denitrification zones and 1‰ in the North Pacific (Figure 9). This amplitude is consistent with the observations which show amplitudes of up to 2‰ close to denitrification zones (e.g., in the Arabian Sea, Figure 1c) and amplitudes of around 1‰ at sites farther downstream (e.g., along the California Current, Figure 1a). In the southeast Pacific south of 30°S the amplitude is smaller than 1‰ suggesting that other processes that are not considered in the model contribute to the observed changes there [Robinson *et al.*, 2007].

## 7. Discussion and Conclusions

[22] Our simulations show that changes in the buoyancy-driven ocean circulation associated with a reduction of NADW have a large effect on subsurface oxygen concentrations in the Indian and Pacific oceans. Additional sensitivity experiments that address the influence of changes in wind stress and North Pacific Intermediate Water formation on the stadial-interstadial oxygen fluctuations indicate that these effects are also significant, but somewhat smaller than the changes brought about by the thermohaline circulation. However, owing to the simplified treatment of the effect of wind changes though our asynchronous coupling strategy this only presents a first-order assessment of changes in

ocean circulation due to changes in momentum transfer. Not considered in our experiments were changes in atmospheric advective transport of heat and moisture and their influence on the buoyancy fluxes. Therefore it will be highly desirable to test if our results are robust in synchronously coupled atmosphere-ocean general circulation models. The amplitude of the atmospheric wind stress response is larger in higher-resolution models (compare e.g., the  $3.75^\circ \times 3.75^\circ$  GENESIS with the  $2^\circ \times 2.5^\circ$  CM2.0 GFDL model in Figure 8) and might still be underestimated by the GFDL model. Thus higher-resolution simulations are needed to test convergence of results with resolution.

[23] A weakness of the model is its simulation of equatorial dynamics. The equatorial undercurrent (EUC) which delivers oxygenated waters and nutrients [Tsuchiya, 1981; Toggweiler and Carson, 1995] from the western tropical Pacific to the margins of North and South America, is typically underestimated in coarse resolution models [Toggweiler *et al.*, 1991; Aumont *et al.*, 1999; Large *et al.*, 2001]. Hence the extent of the suboxic zones is overestimated and one large suboxic water mass centered along the equator is simulated in contrast to the real world, in which two suboxic water masses displaced north and south of the equator are separated by higher oxygen waters along the equator (Figure 2). In the default version of the UVic model maximum zonal velocities in the EUC core are only  $10 \text{ cm s}^{-1}$  and thus underestimated by 1 order of magnitude compared to observations and high-resolution models ( $\sim 1 \text{ m s}^{-1}$  [e.g., Behringer *et al.*, 1998; Lu *et al.*, 1998]). Thus our simulations of denitrification and suboxic zones are subject to uncertainty and should be regarded only as a first coarse estimate. They need to be repeated with a model with improved representation of equatorial dynamics and suboxia. Another uncertainty is associated with the simulated nutrient delivery into the low-latitude thermocline. Several studies [Toggweiler *et al.*, 1991; Toggweiler and Carson, 1995; Sarmiento *et al.*, 2004] suggest that tropical Pacific nutrients are mainly supplied through Subantarctic Mode Water (SAMW), which originates in the Southern Ocean, flows north in the South Pacific and enters the EUC in the western tropical Pacific. Many coarse resolution ocean circulation models, on the other hand, simulate excessive upwelling of deep water at low latitudes, supplying the low-latitude euphotic zone with nutrients though this pathway rather than via SAMW [Toggweiler *et al.*, 1991]. This is particularly the case in models with high diapycnal mixing in the pycnocline [Gnanadesikan, 1999]. In contrast, the model version we used here has low diapycnal diffusion in the pelagic pycnocline ( $2 \cdot 10^{-5} \text{ m}^2 \text{ s}^{-1}$ ) and its simulated ventilation of the upper and intermediate ocean is consistent with observed distributions of radiocarbon, CFCs and other tracers (A. Schmittner *et al.*, Future changes in climate, ocean circulation, ecosystems and biogeochemical cycling simulated for a business-as-usual  $\text{CO}_2$  emission scenario until year 4000 AD, submitted to *Global Biogeochemical Cycles*, 1997, hereinafter referred to as Schmittner *et al.*, submitted manuscript, 2007).

[24] As a result, only about one third (4 Sv) of North Atlantic Deep Water (after being transformed to Circumpo-

lar Deep Water in the Southern Ocean and flowing into the Indian and Pacific oceans) upwells at low latitudes in this model, whereas most NADW (10 Sv) returns to the surface in the Southern Ocean [Schmittner, 2005]. If sinking in the North Atlantic is suppressed in the model, this upwelling and corresponding nutrient delivery to the Southern Ocean surface is reduced, causing a decrease in nutrient concentrations in the area of SAMW formation [see Schmittner, 2005, Figure 3g] and hence reducing nutrient delivery to the tropics via SAMW. Direct upwelling of deep water at low latitudes is also reduced when NADW is suppressed in the model, adding to the decline in nutrient supply and productivity there. We acknowledge, however, that the complex dynamics of Southern Ocean circulation may not be well resolved in this model, and that additional processes there may modulate the North Atlantic-driven signal we have focused on here.

[25] The results shown in this paper have all been performed by a model with preindustrial background climate. We have repeated some experiments with a model version with a colder (glacial) background climate (not shown) which confirm the results reported above and suggest they are robust also for a glacial climate.

[26] In summary, our results demonstrate that changes in the buoyancy-driven ocean circulation alter the fertility of the surface ocean, causing strong variations of export production, subsurface oxygen concentrations and denitrification intensity over broad geographic regions and with very little time lag. Changes in wind-driven upwelling represent a secondary source of variability only. Our findings suggest that ocean ecosystems and biogeochemical cycles respond sensitively to changes in circulation similar to those projected by climate models to occur in the future. Indeed, such changes may already be underway: the buoyancy contrast between surface and upper intermediate waters has been increasing over large swaths of the ocean over the last several years, a likely consequence of warming surface waters. Net primary production estimated for these regions from satellite-based determinations of chlorophyll content imply that export production is decreasing as a result of the diminishing nutrient input to the upper ocean that is, in turn, a consequence of the increased stratification [Behrenfeld *et al.*, 2006].

## Appendix A: Model Description

[27] The physical model is based on the University of Victoria Earth System Climate Model [Weaver *et al.*, 2001] version 2.7. Briefly, it includes a global, three dimensional ocean model with tidal mixing scheme and low diapycnal mixing in the pycnocline with diffusivities in the open ocean of  $2 \cdot 10^{-5} \text{ m}^2 \text{ s}^{-1}$ . It also includes a state of the art dynamic-thermodynamic sea ice model and a simple, two dimensional energy balance model of the atmosphere with prescribed winds. A detailed description and evaluation against observations of the model version used here can be found elsewhere (Schmittner *et al.*, submitted manuscript, 2007).

[28] The marine ecosystem model (Figure A1) is an improved version of Schmittner *et al.* [2005b] and includes

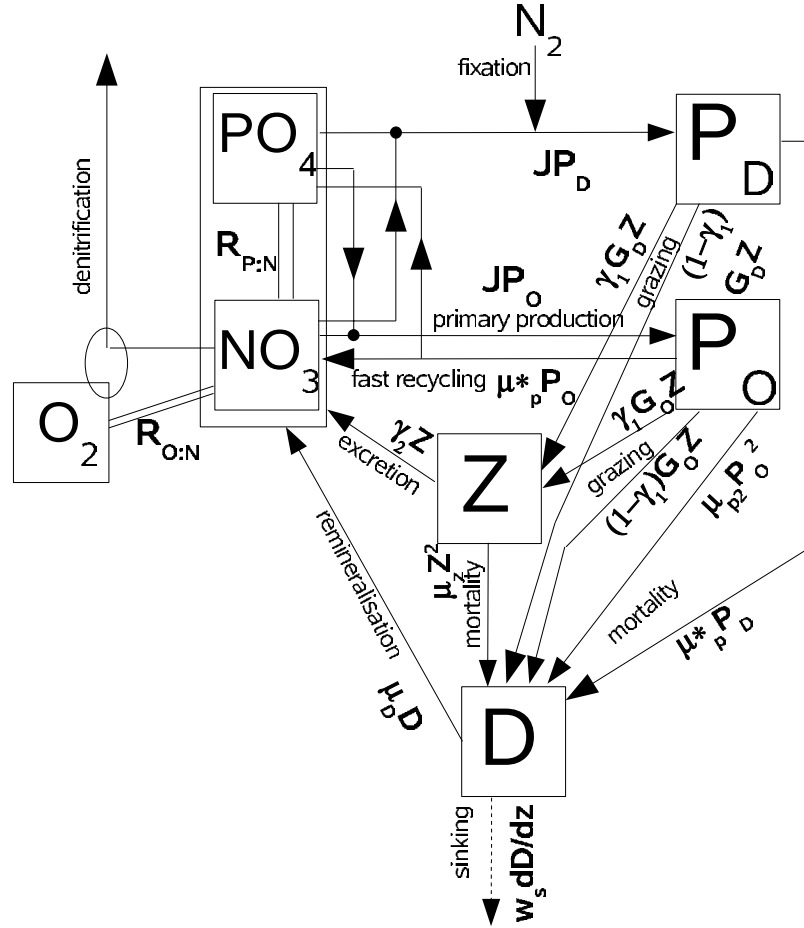


**Figure A1.** Schematic of ecosystem model compartments and interactions. See text for explanation.

interactive cycling of nitrogen, phosphorous and oxygen. It is based on seven prognostic variables and embedded within the ocean circulation model. The inorganic variables include oxygen ( $O_2$ ) and two nutrients, nitrate ( $NO_3$ ) and phosphate ( $PO_4$ ), which are linked through exchanges with the biological variables by Redfield stoichiometry ( $R_{P:N} = 1/16$ ,  $R_{O:N} = 170/16$ ,  $R_{O:P} = 170$ ). The biological variables include two classes of phytoplankton, nitrogen-fixing Diazotrophs ( $P_D$ ), and other phytoplankton ( $P_O$ ), as well as zooplankton ( $Z$ ) and particulate detritus ( $D$ ); all biological variables are expressed in units of mmol nitrogen per  $m^3$ . Although very simple, this ecological structure captures the essential dynamic of competition for phosphorus highlighted by Tyrell [1999], in which phytoplankton capable of rapid growth using available nutrients ( $P_O$ ) are pitted against slow growers capable of fixing their own supply of nitrogen ( $P_D$ ).

[29] Each variable changes its concentration  $C$  according to the following equation:

$$\frac{\partial C}{\partial t} = T + S, \quad (A1)$$

where  $T$  represents all transport terms including advection, isopycnal and diapycnal diffusion, and convection.  $S$

denotes the source minus sink terms, which describe the biogeochemical interactions as follows:

$$S(PO_4) = (\mu_D D + \mu_P^* P_O + \gamma_2 Z - J_O P_O - J_D P_D) R_{P:N} \quad (A2)$$

$$S(NO_3) = (\mu_D D + \mu_P^* P_O + \gamma_2 Z - J_O P_O - \mu_N J_D P_D) \cdot (1 - 0.8 R_{O:N} r_{sox}^{NO_3}) \quad (A3)$$

$$S(P_O) = J_O P_O - \mu_P^* P_O - G(P_O) Z - \mu_{P_2} P_O^2 \quad (A4)$$

$$S(P_D) = J_D P_D - G(P_D) Z - \mu_P P_D \quad (A5)$$

$$S(Z) = \gamma_1 [G(P_O) + G(P_D)] Z - \gamma_2 Z - \mu_Z Z^2 \quad (A6)$$

$$S(D) = (1 - \gamma_1) [G(P_O) + G(P_D)] Z + \mu_P P_D + \mu_{P_2} P_O^2 + \mu_Z Z^2 - \mu_D D - w_D \partial D / \partial z \quad (A7)$$

$$S(O_2) = F_{sfc} - S(PO_4) R_{O:P} r_{sox}^{O_2} \quad (A8)$$



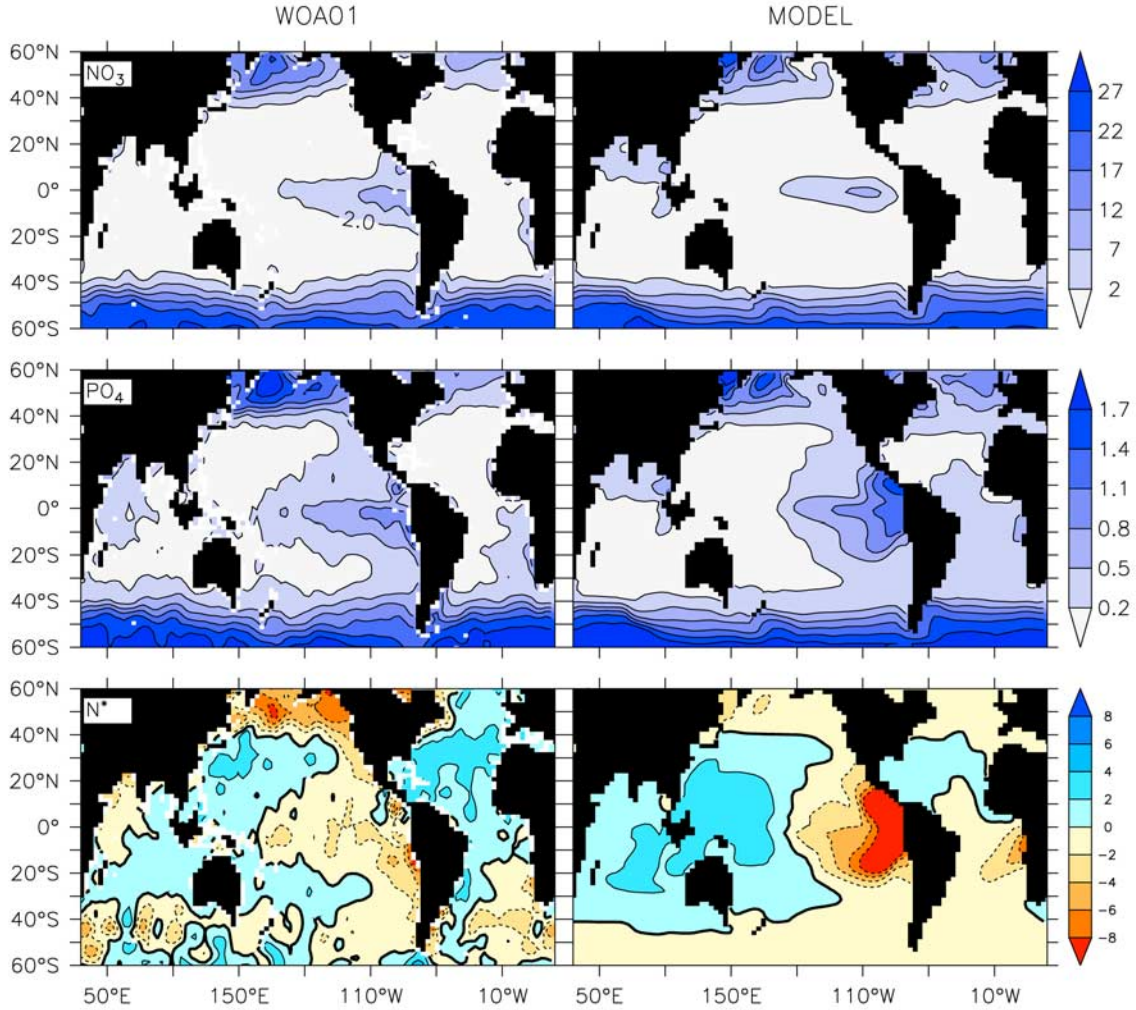


**Figure A2.** (right) Surface distributions of nutrients in the control simulation compared to (left) observations from the World Ocean Atlas 2001.  $N^* = NO_3 - 16 \cdot PO_4 + 3$  indicates the influence of denitrification and nitrogen fixation [Gruber and Sarmiento, 1997]. Units are  $mmol m^{-3}$ . The model captures the major features of the observed surface nutrient distributions such as high values at high latitudes and in the eastern equatorial Pacific. Denitrification in the eastern equatorial Pacific is overestimated as indicated by too low values of  $N^*$ . However, the general distribution of  $N^*$  in the observations, e.g., higher values in the warm pool of the west Pacific and east Indian Ocean as well as in the subtropical North Atlantic and lower values in the east and North Pacific and Southern Ocean, are reproduced by the model.

Grazing of phytoplankton by zooplankton is denoted by  $G(P_x)$  and calculated as described by Schmittner *et al.* [2005b]. The fraction  $\gamma_1$  is ingested, whereas  $(1 - \gamma_1)$  represents sloppy feeding, which is directly converted to detritus. The function  $J_O = J(I, NO_3, PO_4)$  provides the photosynthetic growth rate of nondiazotrophic phytoplankton, determined from irradiance ( $I$ ),  $NO_3$  and  $PO_4$ ,

$$J(I, NO_3, PO_4) = \min(J_{OI}, J_{Omax}u_N, J_{Omax}u_P), \quad (A9)$$

The maximum, nonlimited growth rate is dependent on temperature ( $T$ ):

$$J_{Omax} = ab^{cT} \quad (A10)$$

such that growth rates increase by a factor of ten over the temperature range of  $-2^\circ$  to  $34^\circ C$ . We use  $a = 0.11 \text{ day}^{-1}$  for the maximum growth rate at  $0^\circ C$  which was tuned to optimize surface nutrient concentrations. Under nutrient-replete conditions, the light-limited growth rate  $J_{OI}$  is calculated according to

$$J_{OI} = \frac{J_{Omax}\alpha I}{[J_{Omax}^2 + (\alpha I)^2]^{1/2}} \quad (A11)$$

where  $\alpha$  is the initial slope of the photosynthesis versus irradiance (P-I) curve. The calculation of the photosynthetically active shortwave radiation  $I$  and the method of averaging equation (A13) over one day is given by

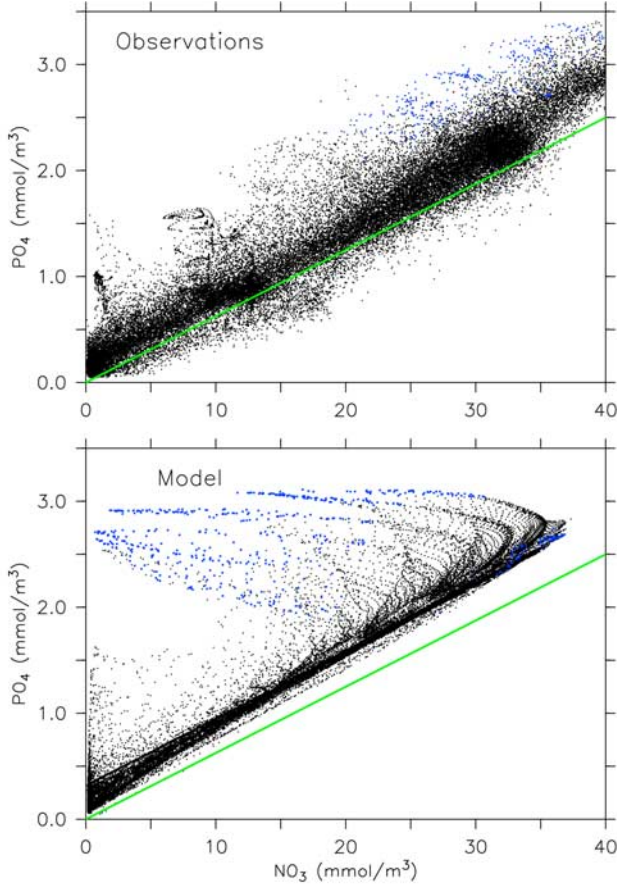


**Figure A3.** Nitrate versus phosphate from (top) observations interpolated on the model grid and from (bottom) the control simulation of the model. The green line corresponds to  $N^* = 3$ . Blue symbols denote suboxic water ( $O_2 < 10 \mu\text{M}$ ). The good linear correlation between  $\text{NO}_3$  and  $\text{PO}_4$  in the observations is well reproduced by the model as well as the fact that most grid points have a lower  $N^*$  than 3 (above the green line). Owing to overestimated denitrification in the model some grid points display very low  $N^*$ , which is not observed in the real ocean.

Schmittner *et al.* [2005b]. Nutrient limitation is represented by the product of  $J_{O_{\max}}$  and the nutrient uptake rates,  $u_N = \text{NO}_3 / (k_N + \text{NO}_3)$  and  $u_P = \text{PO}_4 / (k_P + \text{PO}_4)$  providing the respective nutrient uptake rates.

[30] Diazotrophs grow according to the same principles as the other phytoplankton, but are disadvantaged in nitrate-bearing waters by a lower maximum growth rate,  $J_{D_{\max}}$ , which is zero below  $15^\circ\text{C}$ :

$$J_{D_{\max}} = c_D \max[0, a(b^{cT} - b^{c15^\circ\text{C}})] \quad (\text{A12})$$

The coefficient  $c_D$  handicaps diazotrophs by dampening the increase of their maximal growth rate versus that of other phytoplankton with rising temperature. We use  $c_D = 0.5$ ,

such that the increase per  $^\circ\text{C}$  warming of diazotrophs is 50% that of other phytoplankton. However, diazotrophs have an advantage in that their growth rate is not limited by  $\text{NO}_3$  concentrations:

$$J_D(I, \text{PO}_4) = \min(J_{DI}, J_{D_{\max}} u_P), \quad (\text{A13})$$

although they do take up  $\text{NO}_3$  if it is available (see term 5 in the right-hand side of equation (A3)). The N:P of model diazotrophs is equal to other phytoplankton (16:1). Although there is evidence that the best studied diazotrophs of the genus *Trichodesmium* can have much higher N:P [e.g., Sanudo-Wilhelmy *et al.*, 2004], the more abundant unicellular diazotrophs are uncharacterized [Montoya *et al.*, 2002] and for simplicity of interpretation we opted to keep the N:P of both phytoplankton groups identical.

[31] The first-order mortality rate of phytoplankton is linearly dependent on their concentration,  $P_O$ . DOM and the microbial loop are folded into a single fast remineralization process, which is the product of  $P_O$  and the temperature-dependent term  $\mu^*_P = \mu_P \cdot b^{cT}$ . Diazotrophs do not undergo this fast remineralization, but die at a linear rate.

[32] Detritus is generated from sloppy zooplankton feeding and mortality among the three classes of plankton, and is the only component of the ecosystem model to sink. It does so at a speed of

$$w_D = 7 \text{ m d}^{-1} + 4 \times 10^{-2} \text{ d}^{-1} z, \quad (\text{A14})$$

increasing linearly with depth  $z$  from  $7 \text{ m d}^{-1}$  at the surface to  $220 \text{ m d}^{-1}$  at  $5 \text{ km}$  depth, consistent with observations [Berelson, 2002]. The remineralization rate of detritus is temperature-dependent and decreases by a factor of 5 in suboxic waters, as  $O_2$  decreases from  $5 \mu\text{M}$  to  $0 \mu\text{M}$ :

$$\mu_D = \mu_{D0} b^{cT} [0.65 + 0.35 \tanh(O_2 - 6)] \quad (\text{A15})$$

Remineralization returns the N and P content of detritus to  $\text{NO}_3$  and  $\text{PO}_4$ . Photosynthesis produces oxygen, while respiration consumes oxygen, at rates equal to the consumption and remineralization rates of  $\text{PO}_4$ , respectively, multiplied by the constant ratio  $R_{O:P}$ . Dissolved oxygen exchanges with the atmosphere in the surface layer ( $F_{sfc}$ ) according to the OCMIP protocol.

[33] Oxygen consumption in suboxic waters ( $< 5 \mu\text{M}$ ) is inhibited, according to

$$r_{sox}^{O_2} = 0.5 [\tanh(O_2 - 5) + 1] \quad (\text{A16})$$

but is replaced by the oxygen-equivalent oxidation of nitrate,

$$r_{sox}^{NO_3} = 0.5 [1 - \tanh(O_2 - 5)]. \quad (\text{A17})$$

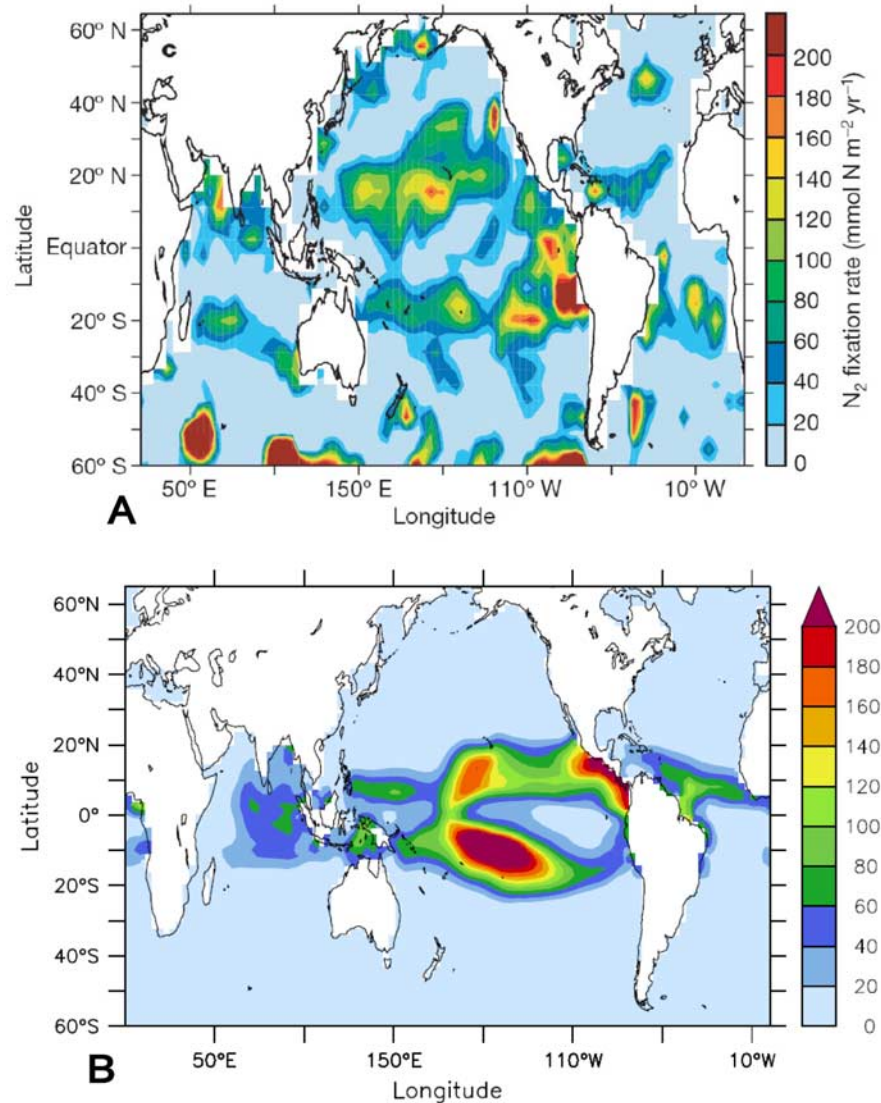


**Figure A4.** Nitrogen fixation (vertically integrated, in  $\text{mmol N m}^{-2} \text{yr}^{-1}$ ) as estimated from (a) observations [Deutsch *et al.*, 2007] and as simulated by (b) the model.

Denitrification consumes nitrate at a rate of 80% of the oxygen equivalent rate, as  $\text{NO}_3^-$  is a more efficient oxidant on a mol per mol basis (i.e., one mol of  $\text{NO}_3^-$  can accept  $5e^-$  while 1 mol of  $\text{O}_2$  can accept only  $4e^-$ ). Note that the model does not include sedimentary denitrification, which would provide a large and less time-variant sink for fixed nitrogen. Because sedimentary denitrification would not change the qualitative dynamics of the model's behavior, but would slow the integration time, it is not included in the version presented here.

[34] The model is integrated for several thousand years until it approaches equilibrium. The global nitrate inventory is variable and its equilibrium value depends on the growth rates of diazotrophs (not shown). The model captures the basic features of the observed phosphate versus nitrate

distributions (Figures A2 and A3). The distribution of diazotrophs (Figure A4) is reasonably consistent with observations and similar to the more complex model of Moore *et al.* [2004]. The pattern and strength of nitrogen fixation in the Pacific is similar to observation-based estimates [Deutsch *et al.*, 2001, 2007] with maxima in the northern and southern tropical/subtropical Pacific and a minimum along the equator. In summary, despite a few shortcomings, the model represents major features of the observed oxygen, phosphate and nitrate distributions.

[35] **Acknowledgments.** Reviews by Robbie Toggweiler and an anonymous referee were appreciated. A.S. and S.H. were supported by the paleoclimate program of the National Science Foundation as part of the PALEOVAR project (ATM-0602395).



## References

- Altabet, M. A., M. J. Higginson, and D. W. Murray (2002), The effect of millennial-scale changes in Arabian Sea denitrification on atmospheric CO<sub>2</sub>, *Nature*, **415**, 159–162.
- Aumont, O., J. C. Orr, P. Monfray, G. Madec, and E. Maier-Reimer (1999), Nutrient trapping in the equatorial Pacific: The ocean circulation solution, *Global Biogeochem. Cycles*, **13**, 351–369.
- Behl, R. J., and J. P. Kennett (1996), Brief interstadial events in the Santa Barbara basin, NE Pacific, during the past 60 kyr, *Nature*, **379**, 243–246.
- Behrenfeld, M. J., R. T. O'Malley, D. A. Siegel, C. R. McClain, J. L. Sarmiento, G. C. Feldman, A. J. Milligan, P. G. Falkowski, R. M. Letelier, and E. S. Boss (2006), Climate-driven trends in contemporary ocean productivity, *Nature*, **444**, 752–755.
- Behringer, D. W., M. Ji, and A. Leetmaa (1998), An improved coupled model for ENSO prediction and implications for ocean initialization. Part I: The ocean data assimilation system, *Mon. Weather Rev.*, **126**(4), 1013–1021.
- Berelson, W. M. (2002), Particle settling rates increase with depth in the ocean, *Deep Sea Res., Part II*, **49**, 237–251.
- Bond, G., W. S. Broecker, S. J. Johnsen, J. McManus, L. Labeyrie, J. Jouzel, and G. Bonani (1993), Correlations between climate records from North Atlantic sediments and Greenland ice, *Nature*, **365**, 143–147.
- Broecker, W. S., D. R. Peteet, and D. Rind (1985), Does the ocean-atmosphere system have more than one stable model of operation?, *Nature*, **315**, 21–26.
- Bryan, F. (1986), High-latitude salinity effects and interhemispheric thermohaline circulations, *Nature*, **323**, 301–304.
- Bryden, H. L., H. R. Longworth, and S. A. Cunningham (2005), Slowing of the Atlantic meridional overturning circulation at 25°N, *Nature*, **438**, 655–657, doi:10.1038/nature04385.
- Cannariato, K. G., and J. P. Kennett (1999), Climatically related millennial-scale fluctuations in strength of California margin oxygen-minimum zone during the past 60 k.y., *Geology*, **27**, 975–978.
- Charles, C. D., and R. G. Fairbanks (1992), Evidence from Southern Ocean sediments for the effect of North Atlantic deep-water flux on climate, *Nature*, **355**, 416–418.
- Crusius, J., T. F. Pedersen, S. Kienast, L. Keigwin, and L. Labeyrie (2004), Influence of northwest Pacific productivity on North Pacific Intermediate Water oxygen concentrations during the Bølling-Allerød interval (14.7–12.9 ka), *Geology*, **32**, 633–636.
- Dansgaard, W., H. B. Clausen, N. Gundestrup, C. U. Hammer, S. F. Johnsen, P. M. Kristinsdottir, and N. Reeh (1982), A new Greenland deep ice core, *Science*, **218**, 1273–1277.
- Deutsch, C., N. Gruber, R. M. Key, J. L. Sarmiento, and A. Ganachaud (2001), Denitrification and N<sub>2</sub> fixation in the Pacific Ocean, *Global Biogeochem. Cycles*, **15**, 483–506.
- Deutsch, C., J. L. Sarmiento, D. M. Sigman, N. Gruber, and J. P. Dunne (2007), Spatial coupling of nitrogen inputs and losses in the ocean, *Nature*, **445**, 163–167.
- Flueckiger, J., T. Blunier, B. Stauffer, J. Chappellaz, R. Spahni, K. Kawamura, J. Schwander, T. F. Stocker, and D. Dahl-Jensen (2004), N<sub>2</sub>O and CH<sub>4</sub> variations during the last glacial epoch: Insight into global processes, *Global Biogeochem. Cycles*, **18**, GB1020, doi:10.1029/2003GB002122.
- Ganeshram, R. S., S. E. Calvert, T. F. Pedersen, and G. L. Cowie (1999), Factors controlling the burial of organic carbon in laminated and bioturbated sediments off NW Mexico: Implications for hydrocarbon preservation—Causes and consequences, *Geochim. Cosmochim. Acta*, **63**, 1723–1734.
- Gnanadesikan, A. (1999), A simple predictive model for the structure of the oceanic pycnocline, *Science*, **283**, 2077–2079.
- Gruber, N. (2004), The dynamics of the marine nitrogen cycle and its influence on atmospheric CO<sub>2</sub>, in *Carbon-Climate Interactions*, NATO ASI Ser., edited by M. Follows and T. Oguz, pp. 97–148, Kluwer Academic, Dordrecht, Netherlands.
- Gruber, N., and J. L. Sarmiento (1997), Global patterns of marine nitrogen fixation and denitrification, *Global Biogeochem. Cycles*, **11**, 235–266.
- Hendy, I. L., and J. P. Kennett (2003), Tropical forcing of North Pacific intermediate water distribution during late Quaternary rapid climate change?, *Quat. Sci. Rev.*, **22**, 673–689.
- Hendy, I. L., T. F. Pedersen, J. P. Kennett, and R. Tada (2004), Intermittent existence of a southern Californian upwelling cell during submillennial climate change of the last 60 kyr, *Paleoceanography*, **19**, PA3007, doi:10.1029/2003PA000965.
- Higginson, M. J., M. A. Altabet, D. W. Murray, R. W. Murray, and T. D. Herbert (2004), Geochemical evidence for abrupt changes in relative strength of the Arabian monsoons during a stadial/interstadial climate transition, *Geochim. Cosmochim. Acta*, **68**, 3807–3826.
- Ivanochko, T. S., R. S. Ganeshram, G.-J. A. Brummer, G. Ganssen, S. J. A. Jung, S. G. Moreton, and D. Kroon (2005), Variations in tropical convection as an amplifier of global climate change at the millennial scale, *Earth Planet. Sci. Lett.*, **235**, 302–314.
- Keigwin, L. D. (1998), Glacial-age hydrography of the far northwestern Pacific Ocean, *Paleoceanography*, **13**, 323–339.
- Kennett, J. P., and B. L. Ingram (1995), A 20,000 year record of ocean circulation and climate change in the Santa Barbara basin, *Nature*, **377**, 510–514.
- Kienast, S. S., S. E. Calvert, and T. F. Pedersen (2002), Nitrogen isotope and productivity variations along the northeast Pacific margin over the last 120 kyr: Surface and subsurface paleoceanography, *Paleoceanography*, **17**(4), 1055, doi:10.1029/2001PA000650.
- Large, W. G., G. Danabasoglu, J. C. McWilliams, P. R. Gent, and F. O. Bryan (2001), Equatorial circulation of a global ocean climate model with anisotropic horizontal viscosity, *J. Phys. Oceanogr.*, **31**, 518–536.
- Levitus, S., and T. P. Boyer (1994), *World Ocean Atlas 1994*, vol. 2, *Oxygen*, NOAA Atlas NESDIS, vol. 2, 202 pp. NOAA, Silver Spring, Md.
- Lu, P., J. P. McCreary Jr., and B. A. Klinger (1998), Meridional circulation cells and the source waters of the Pacific Equatorial Undercurrent, *J. Phys. Oceanogr.*, **28**, 62–84.
- Manabe, S., and R. J. Stouffer (1993), Century-scale effects of increased atmospheric CO<sub>2</sub> on the ocean-atmosphere system, *Nature*, **364**, 215–218.
- Martinez, P., F. Lamy, R. R. Robinson, L. Pichevin, and I. Billy (2006), Atypical  $\delta^{15}\text{N}$  variations at the southern boundary of the east Pacific oxygen minimum zone over the last 50 ka, *Quat. Sci. Rev.*, **25**, 3017–3028.
- McKay, J. L., T. F. Pedersen, and J. Southon (2005), Intensification of the oxygen minimum zone in the northeast Pacific off Vancouver Island during the last deglaciation: Ventilation and/or export production?, *Paleoceanography*, **20**, PA4002, doi:10.1029/2003PA000979.
- Meissner, K. J., E. D. Galbraith, and C. Völker (2005), Denitrification under glacial and interglacial conditions: A physical approach, *Paleoceanography*, **20**, PA3001, doi:10.1029/2004PA001083.
- Mikolajewicz, U., T. J. Crowley, A. Schiller, and R. Voss (1997), Modelling teleconnections between the North Atlantic and North Pacific during the Younger Dryas, *Nature*, **378**, 384–387.
- Mikolajewicz, U., M. Groeger, E. Maier-Reimer, G. Schurgers, M. Vizcaino, and A. M. E. Winguth (2007), Long-term effects of anthropogenic CO<sub>2</sub> emissions simulated with a complex earth system model, *Clim. Dyn.*, **28**, 599–633.
- Mix, A. C., D. C. Lund, N. G. Pisias, P. Boden, L. Bornmalm, M. Lyle, and J. Pike (1999), Rapid climate oscillations in the northeast Pacific during the last deglaciation reflect Northern and Southern Hemisphere sources, in *Mechanisms of Global Climate Change at Millennial Time Scales*, *Geophys. Monogr. Ser.*, vol. 112, edited by P. U. Clark, R. S. Webb, and L. D. Keigwin, pp. 127–148, AGU, Washington, D. C.
- Montoya, J. P., E. J. Carpenter, and D. G. Capone (2002), Nitrogen fixation and nitrogen isotope abundances in zooplankton of the oligotrophic North Atlantic, *Limnol. Oceanogr.*, **47**, 1617–1628.
- Moore, J. K., S. C. Doney, and K. Lindsay (2004), Upper ocean ecosystem dynamics and iron cycling in a global three-dimensional model, *Global Biogeochem. Cycles*, **18**, GB4028, doi:10.1029/2004GB002220.
- Oeschger, H., J. Beer, U. Siegenthaler, B. Stauffer, W. Dansgaard, and C. C. Langway (1984), Late glacial climate history from ice cores, in *Climate Processes and Climate Sensitivity*, *Geophys. Monogr. Ser.*, vol. 29, edited by J. E. Hansen and T. Takahashi, pp. 299–306, AGU, Washington, D. C.
- Ortiz, J. D., S. B. O'Connell, J. DelViscio, W. Dean, J. D. Carriquiry, T. Marchitto, Y. Zheng, and A. van Geen (2004), Enhanced marine productivity off western North America during warm climate intervals of the past 52 k.y., *Geology*, **32**, 521–524.
- Piotrowski, A. M., S. L. Goldstein, S. R. Hemming, and R. G. Fairbanks (2005), Temporal relationships of carbon cycling and ocean circulation, *Science*, **307**, 1933–1938.
- Pourmand, A., F. Marcontonio, and H. Schulz (2004), Variations in productivity and eolian fluxes in the northeastern Arabian Sea during the past 110 ka, *Earth Planet. Sci. Lett.*, **221**, 39–54.
- Reichart, G. J., L. J. Lourens, and W. J. Zachariasee (1998), Temporal variability in the northern Arabian Sea Oxygen Minimum Zone (OMZ) during the last 225,000 years, *Paleoceanography*, **13**, 607–621.
- Reichart, G. J., S. J. Schenau, G. J. de Lange, and W. J. Zachariasee (2002), Synchronicity of oxygen minimum zone intensity on the Oman and Pakistan margins at sub-Milankovich time scales, *Mar. Geol.*, **185**, 403–415.
- Reichart, G.-J., H. Brinkhuis, F. Huiskamp, and W. J. Zachariasee (2004), Hyperstratification following glacial overturning events in the



- northern Arabian Sea, *Paleoceanography*, 19, PA2013, doi:10.1029/2003PA000900.
- Robinson, R. S., A. Mix, and P. Martinez (2007), Southern Ocean control on the extent of denitrification in the southeast Pacific over the last 70 ky, *Quat. Sci. Rev.*, 26, 201–212.
- Saenko, O. A., A. Schmittner, and A. J. Weaver (2004), The Atlantic-Pacific seesaw, *J. Clim.*, 17, 2033–2038.
- Sanudo-Wilhelmy, S. A., A. Tovar-Sanchez, F.-X. Fu, D. G. Capone, E. J. Carpenter, and D. A. Hutchins (2004), The impact of surface-adsorbed phosphorus on phytoplankton Redfield stoichiometry, *Nature*, 432, 897–901.
- Sarniento, J. L., N. Gruber, M. A. Brzezinski, and J. P. Dunne (2004), High-latitude controls of thermocline nutrients and low latitude biological productivity, *Nature*, 427, 56–60.
- Sarnthein, M., et al. (2001), Fundamental modes and abrupt changes in the North Atlantic circulation and climate over the last 60 ky—Concepts, reconstruction and numerical modeling, in *The Northern North Atlantic: A Changing Environment*, edited by P. Schaefer et al., pp. 365–410, Springer, New York.
- Sarnthein, M., T. Kiefer, P. M. Grootes, H. Elderfield, and H. Erlenkeuser (2006), Warmings in the far northwestern Pacific promoted pre-Clovis immigration to America during Heinrich event 1, *Geology*, 34, 141–144.
- Schmittner, A. (2005), Decline of the marine ecosystem caused by a reduction in the Atlantic overturning circulation, *Nature*, 443, 628–633.
- Schmittner, A., and A. C. Clement (2002), Sensitivity of the thermohaline circulation to tropical and high latitude freshwater forcing during the last glacial-interglacial cycle, *Paleoceanography*, 17(2), 1017, doi:10.1029/2000PA000591.
- Schmittner, A., O. A. Saenko, and A. J. Weaver (2003), Coupling of the hemispheres in observations and simulations of glacial climate change, *Quat. Sci. Rev.*, 22, 659–671.
- Schmittner, A., M. Latif, and B. Schneider (2005a), Model projections of the North Atlantic thermohaline circulation for the 21st century assessed by observations, *Geophys. Res. Lett.*, 32, L23710, doi:10.1029/2005GL024368.
- Schmittner, A., A. Oschlies, X. Giraud, M. Eby, and H. L. Simmons (2005b), A global model of the marine ecosystem for long-term simulations: Sensitivity to ocean mixing, buoyancy forcing, particle sinking, and dissolved organic matter cycling, *Global Biogeochem. Cycles*, 19, GB3004, doi:10.1029/2004GB002283.
- Schmittner, A., E. J. Brook, and J. Ahn (2007), Impact of the ocean's overturning circulation on atmospheric CO<sub>2</sub>, in *Ocean Circulation: Mechanisms and Impacts*, *Geophys. Monogr. Ser.*, vol. 173, edited by A. Schmittner, J. Chiang, and S. Hemming, AGU, Washington, D. C., in press.
- Schulte, S., F. Rostek, E. Bard, J. Rullkoetter, and O. Marchal (1999), Variations of oxygen-minimum and primary productivity recorded in sediments of the Arabian Seas, *Earth Planet. Sci. Lett.*, 173, 205–221.
- Schulz, H., U. von Rad, and H. Erlenkeuser (1998), Correlation between Arabian Sea and Greenland climate oscillations of the past 110,000 years, *Nature*, 54, 54–57.
- Suthhof, A., V. Ittekkot, and B. Gaye-Haake (2001), Millennial-scale oscillation of denitrification intensity in the Arabian Sea during the late Quaternary and its potential influence on atmospheric N<sub>2</sub>O and global climate, *Global Biogeochem. Cycles*, 15, 637–649.
- Thompson, S. L., and D. Pollard (1997), Greenland and Antarctic mass balances for present and doubled atmospheric CO<sub>2</sub> from the GENESIS version-2 global climate model, *J. Clim.*, 10, 871–900.
- Timmermann, A., U. Krebs, F. Justino, H. Goosse, and T. Ivanochko (2005), Mechanisms for millennial-scale global synchronization during the last glacial period, *Paleoceanography*, 20, PA4008, doi:10.1029/2004PA001090.
- Toggweiler, J. R., K. Dixon, and W. S. Broecker (1991), The Peru upwelling and the ventilation of the South Pacific thermocline, *J. Geophys. Res.*, 96, 20,467–20,497.
- Toggweiler, J. R., and S. Carson (1995), What are upwelling systems contributing to the ocean's carbon and nutrient budgets?, in *Upwelling in the Ocean: Modern Processes and Ancient Records*, edited by C. P. Summerhayes et al., pp. 337–360, John Wiley, Hoboken, N. J.
- Tsuchiya, M. (1981), The origin of the Pacific equatorial 13°C water, *J. Phys. Oceanogr.*, 11, 794–812.
- Tyrell, T. (1999), The relative influence of nitrogen and phosphorus on oceanic primary production, *Nature*, 400, 525–531.
- van Geen, A., Y. Zheng, J. M. Bernhard, K. G. Cannariato, J. Carriquiry, W. E. Dean, B. W. Eakins, J. D. Ortiz, and J. Pike (2003), On the preservation of laminated sediments along the western margin of North America, *Paleoceanography*, 18(4), 1098, doi:10.1029/2003PA000911.
- Voelker, A. (2002), Global distribution of centennial-scale records for marine isotope stage (MIS) 3: A database, *Quat. Sci. Rev.*, 21, 1185–1212.
- Weaver, A. J., et al. (2001), The UVic Earth System Climate Model: Model description, climatology and applications to past, present and future climates, *Atmos. Ocean*, 39, 361–428.
- Zhang, R., and T. L. Delworth (2005), Simulated tropical response to a substantial weakening of the Atlantic thermohaline circulation, *J. Clim.*, 18, 1853–1860.
- Zheng, Y., A. van Geen, R. F. Anderson, J. V. Gardner, and W. E. Dean (2000), Intensification of the northeast Pacific oxygen minimum zone during the Bölling-Alleröd warm period, *Paleoceanography*, 15, 528–536.

E. D. Galbraith, Atmospheric and Oceanic Sciences, Princeton University, 300 Forrester Road, Princeton, NJ 08540, USA.

S. W. Hostetler, Department of Geosciences, Oregon State University, Corvallis, OR 97331, USA.

T. F. Pedersen, School of Earth and Ocean Sciences, University of Victoria, P. O. Box 3055 STN CSC, Victoria, BC, Canada V8W 3P6.

A. Schmittner, College of Oceanic and Atmospheric Sciences, Oregon State University, 104 COAS Administration Bldg., Corvallis, OR 97331-5503, USA. (aschmittner@coas.oregonstate.edu)

R. Zhang, Geophysical Fluid Dynamics Laboratory, Princeton University, 300 Forrester Road, Princeton, NJ 08540, USA.